arXiv:cond-mat/0309171v1 [cond-mat.supr-con] 7 Sep 2003

Effect of an Electron-phonon Interaction on the One-electron Spectral Weight of a d-wave Superconductor

A. W. Sandvik,[1, 2, *] D. J. Scalapino,[2, †] and N.E. Bickers[3, ‡]

[1]*Department of Physics,Åbo Akademi University, Porthansgatan 3, FIN-20500 Turku, Finland*
[2]*Department of Physics, University of California, Santa Barbara, CA 93106-9530*
[3]*Department of Physics, University of Southern California, Los Angeles, CA 90089-0484*

(Dated: February 2, 2008)

Here we analyze the effects of an electron-phonon interaction on the one-electron spectral weight $A(k,\omega)$ of a $d_{x^2-y^2}$ superconductor. We study the case of an Einstein phonon mode with various momentum-dependent electron-phonon couplings and compare the structure produced in $A(k,\omega)$ with that obtained from coupling to the magnetic π-resonant mode. We find that if the strength of the interactions are adjusted to give the same renormalization at the nodal point, the differences in $A(k,\omega)$ are generally small but possibly observable near $k=(\pi,0)$.

PACS numbers: 79.60, 74.72.-h, 74.25.Kc

I. INTRODUCTION

The role of the electron-phonon coupling in the high T_c cuprates remains a puzzle. The initial finding of the absence of a phonon signature in the temperature dependence of the resistivity[1] and the small size of the isotope effect in the optimally doped cuprates[2] suggested that the electron-phonon interaction played a relatively unimportant role in these strongly-correlated materials. However, large isotope effects away from optimal doping,[2,3] significant phonon renormalization induced in the superconducting state,[4,5,6,7] and recent interpretations of ARPES data[8,9] continue to raise questions regarding the nature and role of the electron-phonon interaction in the high T_c cuprates.

One point of view is that the effects of the strong Coulomb interaction act to suppress the electron-phonon interaction and that while the electron-lattice interaction enters the problem, it does so on a secondary level coming along as it were for the ride. For example, in this view the large isotope effects observed in some of the cuprates away from optimal doping arises from the influence of the lattice on stripe fluctuations, acting to stabilize these and thus suppressing superconductivity.[10] Similarly, the superconductivity-induced phonon renormalization and the possible Englesberg-Schrieffer[11] signature in the ARPES data could be interpreted as naturally occurring in an interacting system but having little effect on the underlying superconducting pairing mechanism. Alternatively one might interpret the isotope effect and the phonon renormalization as supporting the existence of a significant electron-phonon coupling. Furthermore, ARPES measurements have been specifically interpreted in terms of phonon modes that could drive $d_{x^2-y^2}$ pairing.[9] Here, we analyze a simple model of an electron-phonon interaction with the goal of obtaining insight into what one expects to see in the ARPES data of a $d_{x^2-y^2}$ superconductor with electron-phonon interactions.

Continuing technological advances along with improved sample quality have allowed angle-resolved photoemission spectroscopy (ARPES) to probe details of the energy and momentum structure of the one-electron excitations in the cuprate materials.[12] Although simplified, the sudden approximation leads to a useful picture in which the ARPES intensity is equal to the square of a matrix element which depends upon the photon energy, polarization, and the sample geometry times a product of the single particle spectral weight

$$A(k,\omega)=\frac{1}{\pi}\,\mathrm{Im}\{G(k,\omega)\} \tag{1}$$

and a Fermi factor $f(\omega)$. Here $G(k,\omega)$ is the one-electron Green's function. Thus, the idea is that from the k and ω dependence of the ARPES data, one can extract information about the spectral weight $A(k,\omega)$. Then, from this, one seeks to learn about the electron self-energy $\Sigma(k,\omega)$ and the structure of the effective interaction. In particular, the role of spin fluctuations and the π-resonance on the superconducting state spectral function have been studied.[13,14,15] With the recent suggestions[8] from ARPES measurements that there may be a significant coupling of the electrons to a phonon with an energy of order 40meV, one would like to understand how this would effect the ARPES spectrum.

From the number of atoms in a unit cell, it is clear that there are a large number of phonon modes in the cuprates. Here we will focus on several of the modes associated with the motion of the O ions. We will treat these as Einstein phonons. Then for a Hubbard-like model in which the Cu sites form the Hubbard lattice, the effective electron-electron interaction is

$$V(q,\omega)=\frac{2|g(q)|^2\Omega_0}{\omega^2-\Omega_0^2+i\delta}. \tag{2}$$

If $|g(q)|^2=|g|^2$ is independent of the momentum transfer, $V(q,\omega)$ does not couple to the $d_{x^2-y^2}$-pairing channel. This could model the coupling to the c-axis vibration of the apical oxygen. Alternatively, if the electron-phonon matrix element is momentum dependent, the interaction given by Eq. (2) can couple to the $d_{x^2-y^2}$-pairing channel.

The possibility that an electron-phonon interaction could give rise to d-wave pairing has been discussed by various authors.[9,16,17,18,19,20,21] In one approach, the d-wave pairing interaction occurs as the result of the interplay of the O half-breathing mode and the exchange interaction.[9] Other approaches suggest that the Coulomb interaction can lead to a peaking of the electron-phonon coupling at small momentum transfers which favors $d_{x^2-y^2}$ pairing.[16,22] This type of momentum dependence also occurs directly for certain phonon modes. For example, for the Cu-O-Cu buckling-like mode[17,18,19,20,21] the square of the electron-phonon coupling constant is

$$|g(q)|^2 = |g|^2 \left(\cos^2\left(\frac{q_x}{2}\right) + \cos^2\left(\frac{q_y}{2}\right)\right). \tag{3}$$

Setting $q = k - k'$, the momentum-dependent part of this coupling factors into a sum of separable terms

$$\begin{aligned} &|g(k-k')|^2 = \\ &|g|^2\Big(1 + \frac{1}{4}(\cos k_x - \cos k_y)(\cos k'_x - \cos k'_y) + \cdots\Big), \end{aligned} \tag{4}$$

including additional $(\cos k_x + \cos k_y)$ and $(\sin k_x \pm \sin k_y)$ factors. The plus sign in front of the d-wave term implies that this type of phonon exchange provides an attractive channel for d-wave pairing. The key point is that if the electron-phonon coupling $|g(k,k')|$ falls off at large $|k-k'|$ momentum transfers, then such a phonon exchange can mediate d-wave pairing.

Alternatively, an in-plane O breathing-like mode has

$$|g(q)|^2 = |g|^2 \left(\sin^2\left(\frac{q_x}{2}\right) + \sin^2\left(\frac{q_y}{2}\right)\right). \tag{5}$$

This increases at large momentum transfers giving rise to a repulsive interaction in the $d_{x^2-y^2}$-channel. Setting $q = k - k'$ in Eq. (5) one finds that

$$\begin{aligned} &|g(k-k')|^2 = \\ &|g|^2\Big(1 - \frac{1}{4}\ (\cos k_x - \cos k_y)(\cos k'_x - \cos k'_y) + \cdots\Big), \end{aligned} \tag{6}$$

and the minus sign in the second term implies that this phonon suppresses d-wave pairing.[17,18,19,20,21]

In Section II we discuss the simplified case of a cylindrical Fermi surface and a separable phonon mediated interaction. This provides insight into the differences between the s-wave and d-wave cases and establishes the structure of the singularities in the self-energy that are reflected in $A(k,\omega)$ for an Einstein mode. While in the actual materials, the singularities are broadened by the dispersion of the phonon mode, quasiparticle lifetime effects due to other interactions and impurities, as well as finite temperature effects, these results provide a useful framework for understanding the structure that appears in $A(k,\omega)$.

In Section III, we include the effects of a $t - t'$ band structure and the momentum dependence of the coupling. We consider the three different electron-phonon coupling constants discussed above and compare these with the response to the π-resonance spin fluctuation mode. The analysis of the π-resonance mode has been extensively discussed in Refs 14,15. Various estimates for the strength of the π-resonance-electron coupling have been made.[23,24] Here, we chose this coupling so that the renormalization of the nodal Fermi velocity is comparable with that obtained for the phonon coupling. Then we compare and discuss the spectral weights for the various modes. Section IV contains a summary of the results and our conclusions.

II. A CYLINDRICAL FERMI SURFACE AND AN EINSTEIN PHONON

In this section we consider the case of a cylindrical Fermi surface and an interaction arising from the exchange of an Einstein phonon of frequency Ω_0

$$V(\theta,\theta',\omega) = \frac{2|g(\theta,\theta')|^2\Omega_0}{\omega^2 - \Omega_0^2 + i\,\delta}. \tag{7}$$

Here, θ and θ' denote different k vectors on the cylindrical Fermi surface. With Eq. (4) in mind, we will take $|g(\theta,\theta')|^2$ to have the separable form

$$|g(\theta,\theta')|^2 = |g_z|^2 + |g_\phi|^2 \cos 2\theta \cos 2\theta'. \tag{8}$$

The one-electron Green's function can be written as

$$G(k,\omega) = \frac{Z(\omega)\,\omega + \epsilon_k}{(Z(\omega)\,\omega)^2 - \epsilon_k^2 - \phi^2(\theta,\omega)}, \tag{9}$$

with $\epsilon_k = k^2/2m - \mu$, $Z(\omega)$ the renormalization parameter and $\phi\,(\theta,\omega) = \phi\,(\omega)\cos(2\theta)$ the gap parameter. The Eliashberg equations for $Z(\omega)$ and $\phi\,(\omega)$ are

$$\begin{aligned} (1 - Z(\omega))\,\omega = \lambda_z \textstyle\int_0^\infty d\omega' \int \frac{d\theta}{2\pi} \\ \mathrm{Re}\left\{\left(\frac{Z(\omega')\,\omega'}{[(Z(\omega')\,\omega')^2 - \phi^2(\omega')\cos^2 2\theta]^{\frac{1}{2}}}\right) \times \right. \\ \left.\left(\frac{1}{\omega'+\omega+\Omega_0 - i\,\delta} - \frac{1}{\omega'-\omega+\Omega_0-i\,\delta}\right)\right\} \end{aligned} \tag{10a}$$

$$\begin{aligned} \phi\,(\omega) = \lambda_\phi \textstyle\int_0^\infty d\omega' \int \frac{d\theta}{2\pi} \\ \mathrm{Re}\left\{\left(\frac{\phi\,(\omega')\cos^2 2\theta}{[(Z(\omega')\omega')^2 - \phi^2(\omega')\cos^2 2\theta]^{\frac{1}{2}}}\right) \times \right. \\ \left.\left(\frac{1}{\omega'+\omega+\Omega_0 - i\,\delta} + \frac{1}{\omega'-\omega+\Omega_0-i\,\delta}\right)\right\}, \end{aligned} \tag{10b}$$

with $\lambda_z = 2|g_q|^2 N(0)/\Omega_0$ and $\lambda_\phi = 2|g_\phi|^2 N(0)/\Omega_0$. Here $N(0)$ is the one-electron density of states at the Fermi surface.

In order to determine the effect of the phonon on $Z(\omega)$ and $\phi\,(\omega)$, we will adapt an approximation used in the early studies of the role of phonons on the superconducting I(V) characteristic.[25] From the form of eqs (10a) and (10b), one sees that there will be structure in $Z(\omega)$ and

$\phi(\omega)$ when $\omega \simeq \pm(\Omega_0 + \Delta(\theta))$. In this case, ω' will be of order the gap $\Delta(\theta)$ at the gap edge

$$\Delta(\theta) = \frac{\phi(\theta, \omega = \Delta(\theta))}{Z(\theta, \omega = \Delta(\theta))}. \tag{11}$$

Therefore, if the low-energy response in the superconducting state is well described in terms of BCS d-wave quasiparticles, one can replace $Z(\omega')$ and $\phi(\theta, \omega')/Z(\omega')$ inside the integrals by $Z(0)$ and $\Delta(\theta) = \Delta_0 \cos 2\theta$. Then, taking the imaginary parts of eqs (10a) and (10b) we have for $\omega > 0$

$$\omega Z_2(\omega) = 4\lambda_z \int_{\theta_c}^{\frac{\pi}{4}} d\theta \frac{(\omega - \Omega_0)}{[(\omega - \Omega_0)^2 - \Delta_0^2 \cos^2 2\theta]^{\frac{1}{2}}} \tag{12a}$$

$$\phi_2(\omega) = 4\lambda_\Delta \int_{\theta_c}^{\frac{\pi}{4}} d\theta \frac{\Delta_0 \cos^2 2\theta}{[(\omega - \Omega_0)^2 - \Delta_0^2 \cos^2 2\theta]^{\frac{1}{2}}} \tag{12b}$$

Here θ_c is such that $\Delta(\theta_c) = \omega - \Omega_0$ and $\phi_2(\omega)$ and $Z_2(\omega)$ are even functions of ω for a time-ordered zero temperature Green's function.

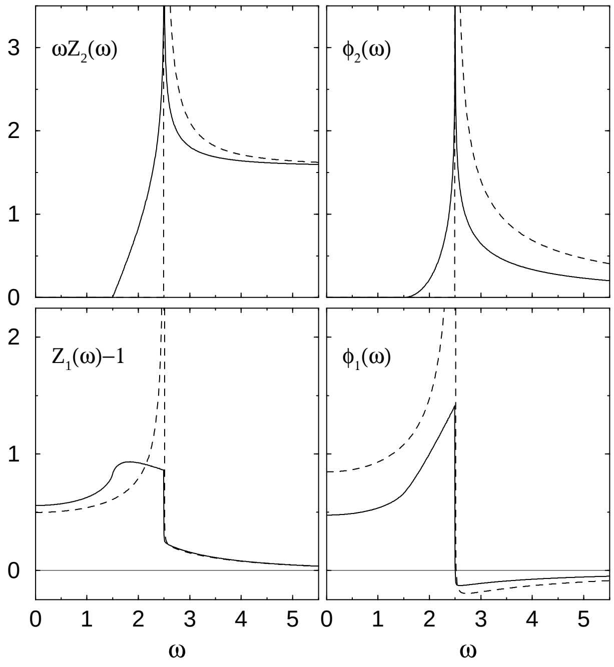

FIG. 1: Results for the real and imaginary phonon-induced contribution to $Z(\omega)$ and $\phi(\omega)$ for a d-wave (solid) and an s-wave (dashed) superconductor. Here we have taken a cylindrical Fermi surface and a separable interaction. $Z(\omega)$ and $\phi(\omega)$ are normalized with respect to the appropriate coupling constant, λ_ϕ and λ_z for the d-wave gap and λ_z for the s-wave case. For all of the circular Fermi surface plots, energy is measured in units of Δ_0 and $\Omega_0 = 1.5\,\Delta_0$. With this normalization $\omega Z_2(\omega)$ goes to $\pi/2$ as $\omega \to \infty$.

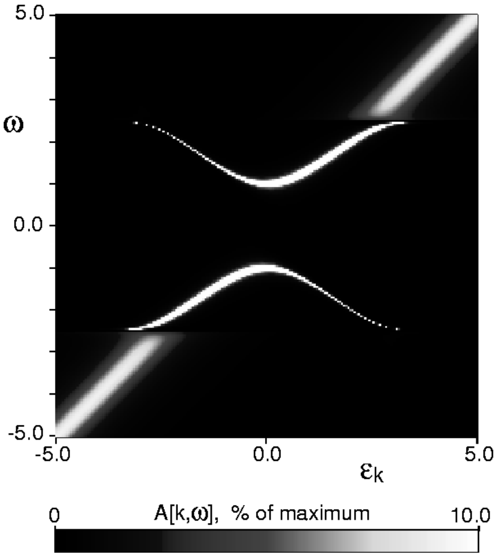

FIG. 2: An intensity plot of the spectral weight $A(k, \omega)$ for the case of an s-wave superconductor coupled to a phonon with frequency Ω_0. As indicated on the color scale, the figure is 'overexposed', i.e. features exceeding 10% of the maximum intensity appear white, in order to show the weaker features.

Results for $\omega Z_2(\omega)$ and $\phi_2(\omega)$ are shown in the top panel of Fig. 1 for both a $d_{x^2-y^2}$-wave and an s-wave gap with $\Omega_0 = 1.5\Delta_0$. For an s-wave gap, $\cos 2\theta$ is set to 1 and $\theta_c = 0$ in eqs (12a) and (12b). For the s-wave case, the imaginary parts of $Z(\omega)$ and $\phi(\omega)$ onset when ω exceeds $\pm\,(\Omega_0 + \Delta_0)$ and exhibit a square root singularity. For a $d_{x^2-y^2}$-gap, these functions onset linearly at $\omega = \pm\,\Omega_0$ because of the gap nodes and there is a log singularity at $\pm\,(\Omega_0 + \Delta_0)$. The real parts of $Z(\omega)$ and $\phi(\omega)$ are obtained from the usual dispersion relations, and results for $Z_1(\omega)$ and $\phi_1(\omega)$ are shown in the lower panel of Fig. 1. For the s-wave case, ϕ_1 and Z_1 exhibit square root singularities as ω approaches $\pm\,(\Omega_0 + \Delta_0)$. This is just the expected Kramers-Kronig transform of the square root singularity in ϕ_2 and Z_2. Similarly, the results for ϕ_1 and Z_1 for the $d_{x^2-y^2}$ case exhibit step discontinuities at $\omega = \pm\,(\Omega_0 + \Delta_0)$ arising from the log singularities in ϕ_2 and Z_2. Naturally in real materials, phonon dispersion, impurity scattering, and finite temperature effects broaden these features. Nevertheless, they provide a simple framework for analyzing the ARPES data.

An intensity plot of $A(k, \omega)$ for the case of an s-wave gap is shown in Fig. 2. Here, $A(k, \omega)$ is obtained from the imaginary part of $G(k, \omega)$, using the s-wave results for $Z(\omega)$ and $\phi(\omega)$ shown in Fig. 1 with $\lambda = 0.5$. The real part of the gap function is supplemented by an additional contribution from an underlying pairing interaction so that the magnitude of the gap at the gap edge is equal to Δ_0. Results for both the ARPES accessible region $\omega \leq 0$ and the inverse photoemission region $\omega > 0$ are shown. The shift of spectral weight due to the quasiparticle coherence factors $\frac{1}{2}(1 + \frac{\epsilon_k}{E_k})$ is clearly seen as is the Englesberg-Schrieffer signature showing the asymptotic approach of a peak in the spectral func-

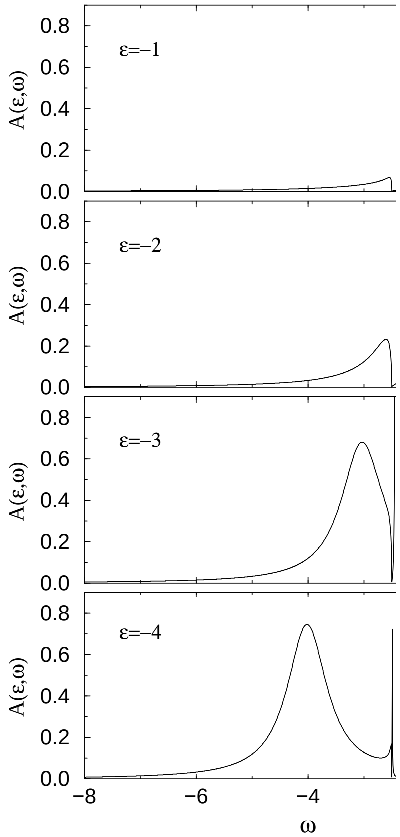

FIG. 3: Energy distribution curves show
ω for various values of ϵ_k for an s-wave su
$\lambda_z = 0.5$. Here one sees that as ϵ_k exceed
peak is left behind whose intensity weake

tion to $\pm\ (\Omega_0 + \Delta_0)$. Because of the
gularity in Z and ϕ, the asymptotic
peak to $\pm\ (\Omega_0 + \Delta_0)$ varies as $(\lambda\Omega_0/\epsilon_k$
the Fermi velocity is renormalized by
that the dispersion of the peak for ω
$\sqrt{(\epsilon_k/Z_1(\Delta_0))^2 + \Delta_0^2}$ while for ω large
a broadened quasiparticle peak dispers
distribution curves (EDC) showing $A($
various values of ϵ_k are shown in Fig.
is the type of EDC that one would ex
traditional s-wave electron-phonon superconductor with a single dominant Einstein mode.[27] More generally, one would have multiple phonon modes and their dispersion along with possible finite temperature effects would lead to a richer response.

Intensity plots of $A(k,\omega)$ for the case of a $d_{x^2-y^2}$ gap are shown in Fig. 4. Just as for the s-wave case, $\phi_1(\theta,\omega)$ is supplemented so that the gap at the gap edge is $\Delta_0 \cos 2\theta$. Fig. 4(a) shows $A(k,\omega)$ for a cut along the antinodal direction in k-space ($\theta = 0$), while Fig. 4(b) shows the results for a cut along the nodal direction ($\theta = \pi/4$). The antinodal cut resembles the s-wave case in the transfer of spectral weight as ϵ_k passes through the Fermi energy and the renormalization of the quasiparticle dispersion. However, the Englesberg-Schrieffer signature no longer asymptotically approaches $\pm\ (\Omega_0 + \Delta_0)$, but rather appears to be broadened and cut off. In the s-wave case, the broadening due to the electron-phonon interaction did not set in until $|\omega|$ exceeded $\Omega_0 + \Delta_0$ leading to the long sweep of the peak which occurs for $|\omega|$ just below $(\Omega_0 + \Delta_0)$. However, the nodal regions associated with a $d_{x^2-y^2}$ gap lead to a finite broadening when $|\omega|$ exceeds Ω_0. The onset of this broadening is seen by the faint horizontal line in Fig. 4 where the intensity changes from black to blue at larger values of ϵ_k. As we will discuss, termination of this peak is a reflection of the fact

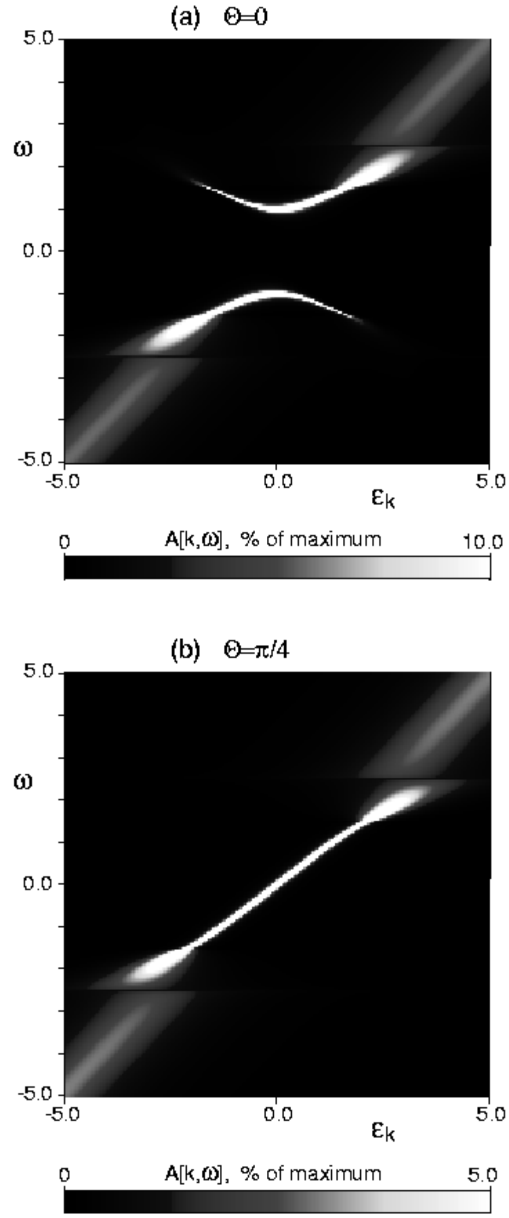

FIG. 4: An intensity plot of $A(k,\omega)$ for a d-wave gap. Results for a $\theta = 0$ cut are shown in (a) and in (b) for $\theta = \pi/4$, a nodal cut.

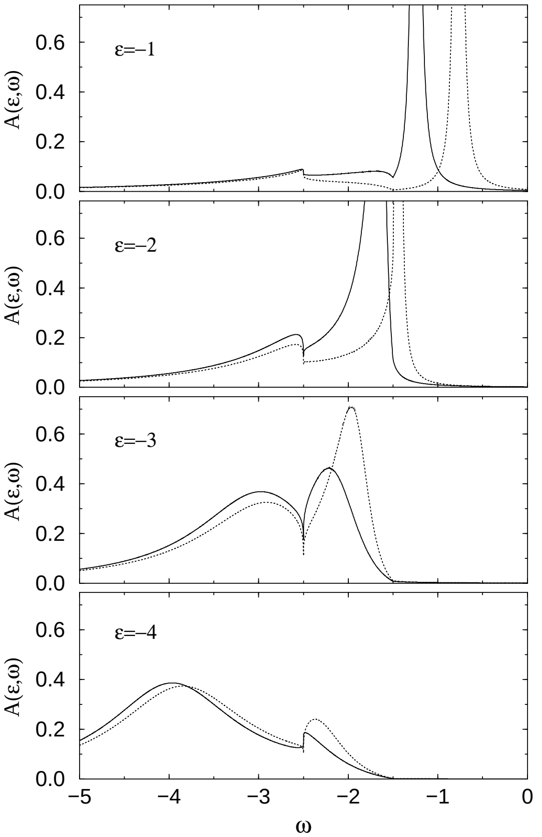

FIG. 5: Energy distribution curves (EDC) showing $A(k,\omega)$ versus ω for different values of ϵ_p with $\lambda_z = \lambda_\phi = 0.5$. Results for the $\theta = 0$ cut are shown as the solid curves and for $\theta = \pi/4$ as the dashed curves.

that for a $d_{x^2-y^2}$-gap, Z_1 and ϕ_1 have step discontinuities at $\pm\,(\Omega_0 + \Delta_0)$ rather than the square root singularities associated with an s-wave gap.

The nodal cut, shown in Fig. 4(b), appears on first glance to be similar to what one would expect for the normal state. That is, a renormalized $\epsilon_k/Z_1(k,0)$ dispersion for $\omega \ll \Omega_0$ with the dispersion returning to its band value ϵ_k for $\omega \gg \Omega_0$. However, the cut-off Englesberg-Schrieffer signature still occurs for $|\omega| = \Omega_0 + \Delta_0$. Thus, the full antinodal gap Δ_0 enters as the characteristic kink energy for all momentum slices. This simply reflects the $|\omega| = \Omega_0 + \Delta_0$ singularities in Z and ϕ shown in Fig. 1. Again, the broadening of the Englesberg-Schrieffer peak when $|\omega|$ exceeds Ω_0 is clearly seen in Fig. 4(b). In Fig. 5, various EDC slices of $A(k,\omega)$ are shown for the $d_{x^2-y^2}$ case. Comparing these with the s-wave case, one sees the broadening and truncation of the Englesberg-Schrieffer lower peak.

The difference in the structure of the Englesberg-Schrieffer signature between the s- and the $d_{x^2-y^2}$-cases can be understood from the plots of

$$\epsilon_k = -\sqrt{(Z_1(\omega)\omega)^2 - \phi_1^2(\omega)} \qquad (13)$$

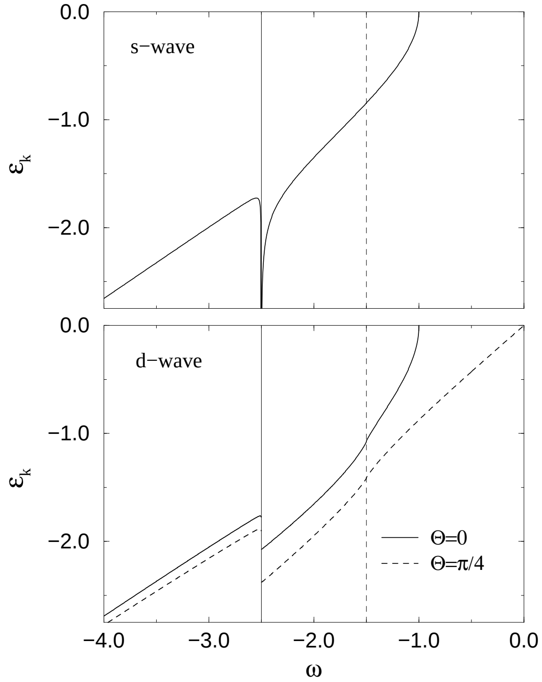

FIG. 6: Plots of $\epsilon_k = -\sqrt{(Z_1(\omega)\omega)^2 - \phi_1^2(\omega,\theta)}$ versus ω along the negative ω axis for $\lambda_\alpha = 0.5$ show the structure of the Englesberg-Schrieffer signature. The upper panel is for an s-wave gap and the lower panel is for a d-wave gap with $\theta = 0$ shown as the solid curve and $\theta = \pi/4$ as the dashed curve.

shown in Fig. 6. One can see that as one probes ϵ_k states which are further below the Fermi energy, two solutions of Eq. (13) develops. For the s-wave case shown in the upper panel of Fig. 6, an undamped lower energy branch asymptotically approaches $\omega = -(\Omega_0+\Delta_0)$, and a second quasiparticle branch at $\omega \simeq -\epsilon_k$ evolves which is damped by the imaginary parts of Z and ϕ. As we have seen, these branches are reflected in the structure of $A(k,\omega)$ and the lower energy branch represents the characteristic Englesberg-Schrieffer signature for an s-wave superconductor. Similar plots for the $d_{x^2-y^2}$-case with $\theta = 0$ and $\theta = \pi/4$ are shown in the lower panel of Fig. 6. Here, unlike the s-wave case, the low energy branch is terminated, reflecting the fact that the singularities in Z_1 and ϕ_1 for the d-wave case are simply step discontinuities at $\pm\,(\Omega_0 + \Delta_0)$. The onset of damping processes for the $d_{x^2-y^2}$ case when $\omega < -\Omega_0$ give rise to the discontinuity in slope seen at $\omega = -\Omega_0$.

III. BAND STRUCTURE AND THE EFFECT OF A MOMENTUM-DEPENDENT COUPLING

We turn next to the effects of the band structure and to the momentum dependence of the electron-phonon coupling. For the band structure, consider a square lattice with a near-neighbor hopping t and a next-near-neighbor hopping t'. In this case

$$\epsilon_k = -2t(\cos k_x + \cos k_y) - 4t' \cos k_x \cos k_y - \mu. \quad (14)$$

For $t'/t = -0.3$ and $\mu/t = -1$, one has the typical Fermi surface shown in Fig. 7 and the single spin electron density of states shown in the inset. We take the gap to be

$$\Delta_k = \Delta_0(\cos k_x - \cos k_y)/2. \quad (15)$$

In this case, the one-electron Green's function can be written in the form

$$G(k,\omega) = \frac{Z(k,\omega)\omega + (\epsilon_k + X(k,\omega))}{(Z(k,\omega)\omega)^2 - (\epsilon_k + X(k,\omega))^2 - \phi^2(k,\omega)}. \quad (16)$$

Adopting the same approximation as before, the phonon-induced contributions to the imaginary parts of the renormalization, energy shift, and gap parameters are given by

$$\begin{aligned} \omega Z_2(k,\omega) &= \frac{\pi}{2N} \sum_{k'} |g(k-k')|^2 \times \\ &\Big(\delta(E_{k'} + \Omega_0 - \omega) - \delta(E_{k'} + \Omega_0 + \omega)\Big), \quad (17a) \end{aligned}$$

$$\begin{aligned} X_2(k,\omega) = -\frac{\pi}{N} \sum_{k'} |g(k-k')|^2 \, \frac{\epsilon_{k'}}{2E_{k'}} \times \\ \Big(\delta\left(E_{k'} + \Omega_0 - \omega\right) + \delta\left(E_{k'} + \Omega_0 + \omega\right)\Big), \quad (17b) \end{aligned}$$

$$\begin{aligned} \phi_2(k,\omega) = \frac{\pi}{N} \sum_{k'} |g(k-k')|^2 \, \frac{\Delta_{k'}}{2E_{k'}} \times \\ \Big(\delta\left(E_{k'} + \Omega_0 - \omega\right) + \delta\left(E_{k'} + \Omega_0 + \omega\right)\Big). \quad (17c) \end{aligned}$$

Here, as before, we assume that an underlying pairing interaction, most likely spin-fluctuations, gives rise to a zero temperature $d_{x^2-y^2}$ superconducting state. At low energies this state is characterized by a renormalized band structure Eq. (14) and chemical potential, a renormalized coupling constant $g(q)$, and a gap given by Eq. (15). These parameters have been used in the Eliashberg equations to describe the state which enters when an excitation at energy $\omega > \Omega_0$ decays to a lower energy $E_{k'}$ state (or when $\omega < -\Omega_0$ decays to $-E_{k'}$). The real parts of $Z(k,\omega)$, $\phi(k,\omega)$, and $X(k,\omega)$ are again found from the Kramer-Kronig dispersion relation. The spectral weight $A(k,\omega)$ is then obtained from Eq. (1) with the chemical potential shift removed from $X_1(k,\omega)$ and a contribution added to the real part of the gap so that the real part of the gap at the gap edge remains equal to Δ_k, Eq. (15). Note that the contributions of the underlying pairing interaction to Z and X, as well as the higher energy part of ϕ, have not been included. Thus, there are additional renormalization and damping effects which do not appear. We basically are seeking to understand the leading contribution of the electron-phonon interaction which is superimposed on top of the other many-body interactions. This approach rests on the idea that in the superconducting state the low-lying electronic states are well described by BCS $d_{x^2-y^2}$ excitations[28] with renormalized band parameters t, t', and μ, a $d_{x^2-y^2}$-wave gap Δ_k, and renormalized electron-phonon coupling constants. Note, that here we are not taking into account the possible change in q-dependence of the electron-phonon couplings produced for example by the Hubbard U.[16,22]

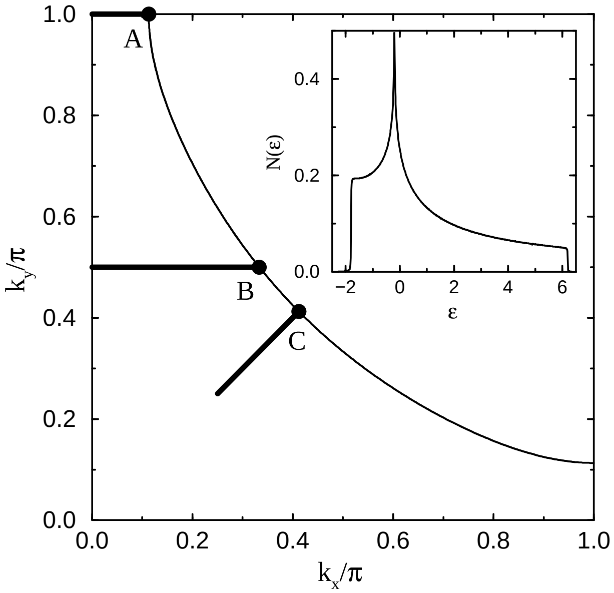

FIG. 7: The Fermi surface for $t'/t = -0.3$ and $\mu = -1$. The inset shows the single spin electron density of states. We will discuss the spectral weight for the cuts marked A, B, and C.

We begin by looking at the self-energy terms for the case of the buckling mode with $|g(q)|^2$ given by Eq. (3) and $|g|^2 = 0.5$ in units of t^{-2}. Results for $\phi(\omega,k)$, $Z(\omega,k)$, and $X(\omega,k)$ are shown in Fig. 8 for k at point A shown in Fig. 7. The imaginary parts of Z and ϕ exhibit the expected log singularity at $\Delta_0 + \Omega_0$ that we previously saw for the case of a circular Fermi surface. In addition, there is a second log singularity at $E(0,\pi) + \Omega_0$ with $E(0,\pi) = \sqrt{\epsilon^2(0,\pi) + \Delta_0^2}$ which comes from the Van Hove singularity[14] at $k = (0,\pi)$. These log singularities in Z_2 and ϕ_2 manifest themselves via the Kramers-Kronig dispersion relation as step-down discontinuities in Z_1 and ϕ_1, as seen in Fig. 8. The energy shift parameter X has only the Van Hove singularity. Naturally, the dispersion of the phonon mode as well as finite temperature and lifetime effects will broaden these features in the actual system. The energy distribution of the spectral weight $A(k,\omega)$ for the buckling mode at momentum k_A is plotted in Fig. 9. It shows the quasiparticle peak at the gap edge Δ_{k_A} as well as structure associated with the buckling phonon at $\Omega_0 + \Delta_0$ and $\Omega_0 + E(0,\pi)$.

As noted in the introduction, one would like to de-

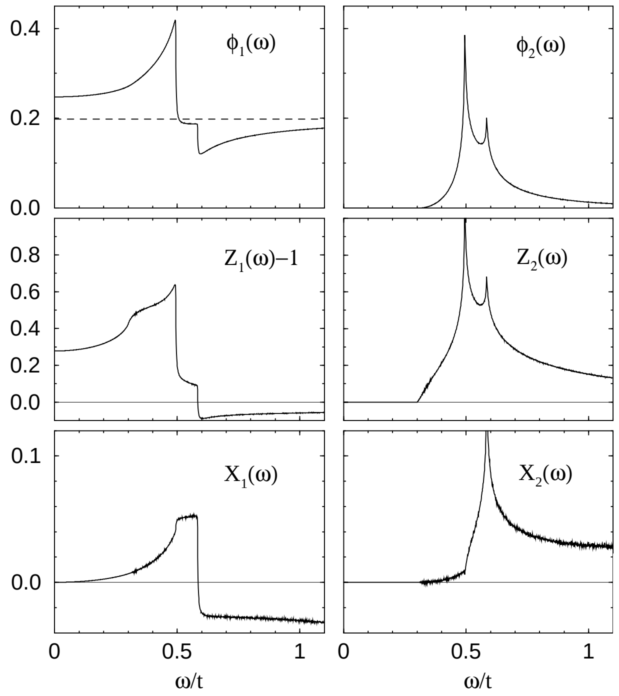

FIG. 8: The self-energy parameters ϕ, Z, and X versus ω f
the case of the buckling phonon coupling, Eq. (3), with $\mathbf{k}$
$\mathbf{k}_A$ corresponding to the point A of Fig. 7. Here $|g|^2 = 0.5$

termine whether the structure observed in the ARPI data is due to phonons or the π-resonance spin fluctu tion mode. Eschrig and Norman[14,15] have analyzed t effect of the π-resonance using a detailed tight binding of the band energy ϵ_k and a coupling to the π-resona mode of frequency Ω_0 given by

$$|g(q)|^2 = g_{SF}^2 \, \frac{w_Q}{1 + 4\xi^2[\cos^2(q_x/2) + \cos^2(q_y/2)]}. \qquad (1$$

Here, we will use the $t - t'$ band structure of Eq. (1 with $t'/t = -0.3$ and $\mu = -1$, set $w_Q = 1$, $\xi = 2$, a set $g_{\rm SF}^2 = 5$ which corresponds to having $\frac{3}{4}(\frac{\bar{U}}{t})^2 =$ in an effective Hubbard RPA interaction. In additic with this choice for $g_{\rm SF}^2$ we will find that $Z_1(k_F, 0)$ the nodal point C is comparable with $Z_1(k_F, 0)$ for t phonons. This makes it convenient for addressing t question of whether there are significant spectral d ferences due simply to the structure of the momentu dependent couplings that would allow one to determi the nature of the mode from the ARPES data.[29] No that for the spin-fluctuation interaction with $|g(q)|^2$ giv by Eq. (18), there is a minus sign on the righthand si of Eq. (17c) for the gap parameter. For the three types phonon couplings we take $|g|^2 = 0.5$ in units of t^{-2}. Tl gives $Z_1(k_F, 0) \simeq 1.3$ corresponding to an effective[30, $\lambda \sim 0.3$. For the π-resonance mode coupling, setting $g_{SF}^2 = 5$ gives $Z_1(k_F, 0) \simeq 1.3$.

Intensity plots of $A(k, \omega)$ for the constant Holstein coupling, the buckling mode coupling Eq. (3), the breathing

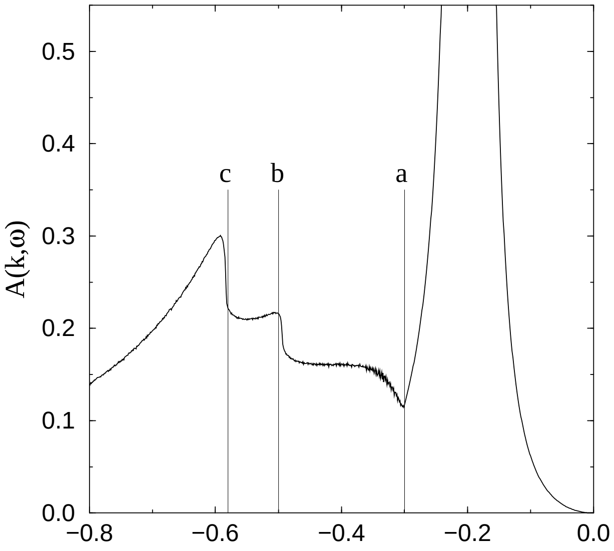

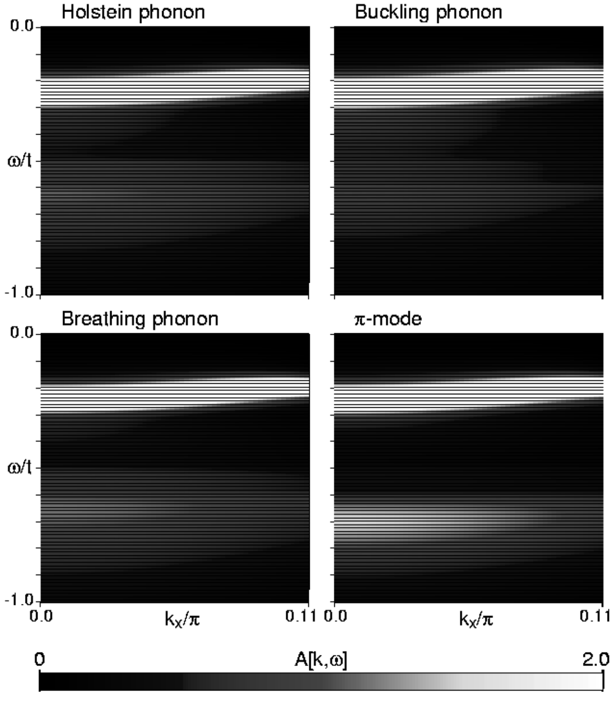

FIG. 10: Intensity plots of $A(k, \omega)$ for the momentum cut A for four different couplings corresponding to the Holstein mode with $|g(q)|^2$ constant, the buckling mode Eq. (3), breathing mode Eq. (5), and π-resonance magnetic mode coupling Eq. (18). Here, $|g|^2 = 0.5$ and $g_{SF}^2 = 5$. The cut-off indicated on the color scale refers to the actual spectral weight intensity (as opposed to the relative scale used in the previous intensity plots) so that one can directly compare the effects of the different couplings.

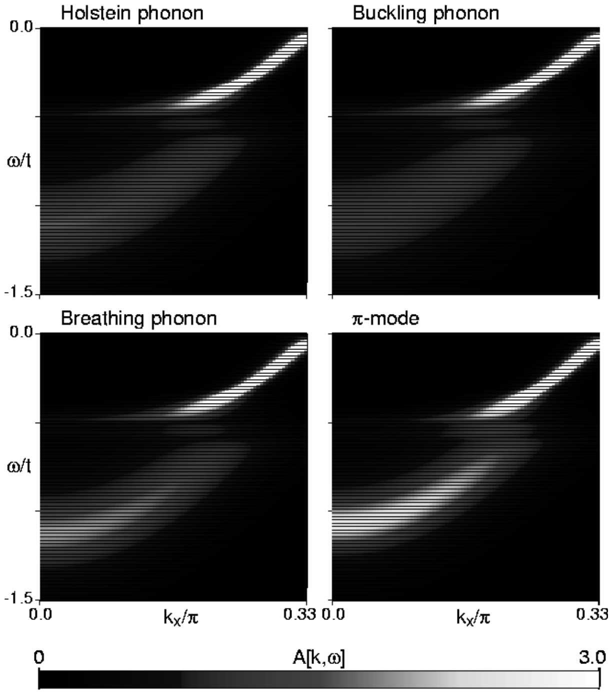

FIG. 11: Intensity plots of $A(k,\omega)$ for the momentum cut for the four different couplings.

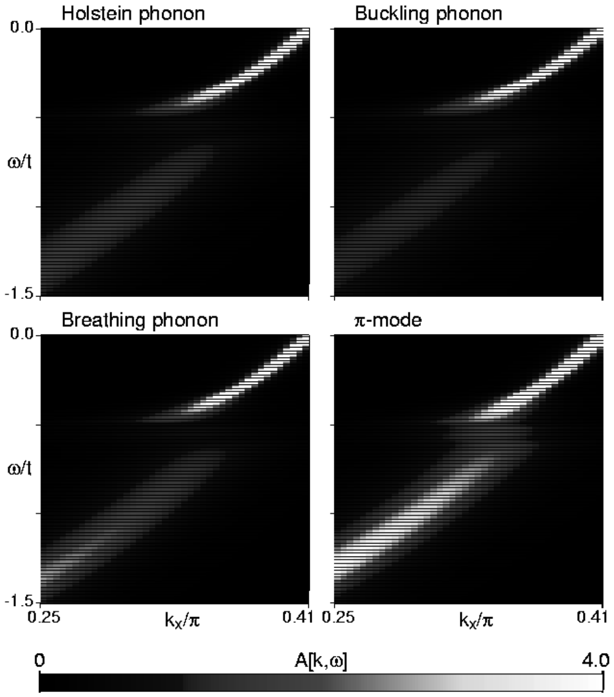

FIG. 12: Intensity plots of $A(k,\omega)$ for the nodal momentum cut C for the four different couplings.

mode coupling Eq. (5), and the π-resonance mode coupling Eq. (18), are shown in Fig. 10 for the momentum cut A. Similar intensity plots for the momentum cuts B and C are shown in Figs 11 and 12. In Fig. 10, one sees a high intensity quasiparticle peak and weaker structures onsetting at $\omega = -(\Omega_0 + \Delta_0)$ and $-(\Omega_0 + E(0,\pi))$ due to the coupling to the phonon or magnetic resonance modes. For the B momentum cut shown in Fig. 11, one can now move deep enough inside the Fermi sea that the Englesberg-Schrieffer lower energy peak (the upper bright curve in the figures) is broadened when ω becomes less than $-\Omega_0$ and terminated at a finite value of k_x as ω approaches $-(\Omega_0 + \Delta_0)$. At still higher energies (ω more negative), a damped quasiparticle branch is seen. The nodal C cut is shown in Fig. 12. Here, one clearly sees the Englesberg-Schrieffer signature with a quasiparticle peak which varies as $\epsilon_k / Z_1(k_F, 0)$ near the Fermi surface, then disperses and bends as ω approaches $-(\Omega_0 + \Delta_0)$. This peak is then terminated as a broadened high energy quasiparticle branch appears at more negative values of ω.

The difference of $A(k,\omega)$ for the various modes is in fact subtle since all four have an Einstein spectrum with $\Omega_0 = 0.3t$, a $d_{x^2-y^2}$ gap with $\Delta_0 = 0.2t$, and a band structure with $t'/t = -0.3$ and $\mu = -1$. Thus, the characteristic energies Δ_0, $\Omega_0 + \Delta_0$, and $\Omega_0 + E(0,\pi)$ are the same. In addition as discussed, we have chosen the coupling constants so that $|g(q)|^2$ averaged over the Brillouin zone is the same for all four cases. Thus, the basic difference is the momentum structure of the dif-

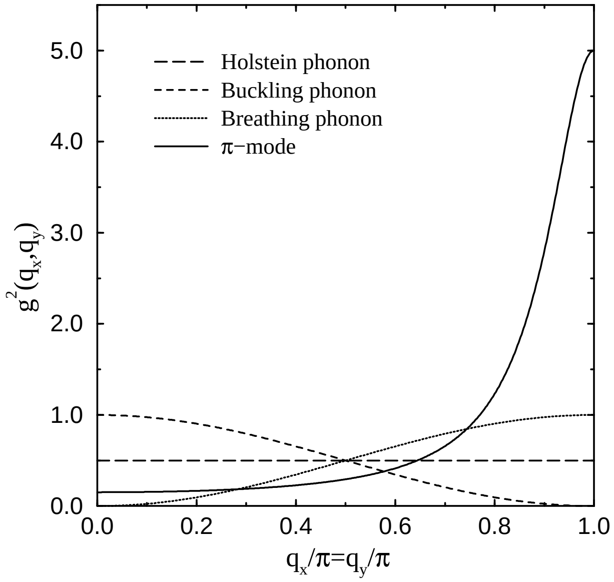

FIG. 13: The momentum dependence of the $|g(q)|^2$ coupling versus $q = q_x = q_y$ for the four different modes with $|g|^2 = 0.5$ for the phonon modes and $g_{SF}^2 = 5$ for the π-mode. Note that this is a slice of a two-dimensional (q_x, q_y) surface and that the volume enclosed by these surfaces is $(2\pi)^2|g|^2$ for each of these couplings.

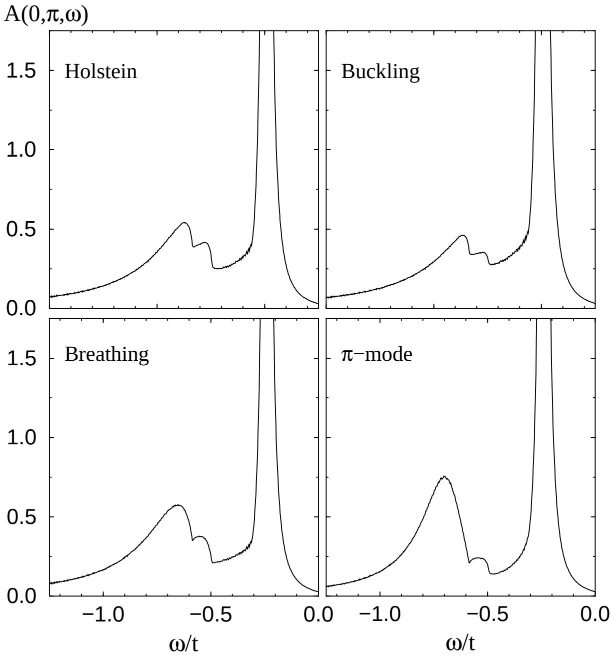

FIG. 14: Energy distribution curves (EDC) showing $A(k,\omega)$ versus ω at $k=(0,\pi)$ for the four different modes.

ferent couplings shown in Fig. 13 for $q_x = q_y$. Here, we see that the spin-fluctuation resonant mode is clearly most strongly peaked at large momentum, followed by the breathing mode phonon, the uniform Holstein coupling, and lastly the buckling mode phonon which has $|g(\pi,\pi)|^2 = 0$. One consequence of the strong peak in the magnetic reasonance-mode coupling is seen in Fig. 10 for the A cut. Here, the increase of the intensity of the spectral weight $A(k,\omega)$ which occurs when ω decreases below $-(\Omega_0 + E(\pi,0))$ is greatest for the spin-fluctuation π-resonance and smallest for the buckling mode.

In Fig. 14 we show the energy distribution curves for the four modes for momentum $k=(0,\pi)$. $A(k,\omega)$ for all of the modes shows a strong peak at Δ_0. For the π-mode, this is followed by a dip and then a secondary peak which develops as ω decreases below the Van Hove threshold at $-(\Omega_0 + E(0,\pi))$. It is this peak-dip-hump structure, for the case in which the effects of the bilayer splitting can be eliminated, that has been identified as a ‘fingerprint’ of the π-resonance.[14,15,32,33] Here, we see that indeed this structure is most pronounced for the π-mode and smallest for the buckling mode. However, this is a quantitative effect rather than a qualitative one and if the phonon coupling increases at large momentum transfers, such as in the case of the breathing mode, this feature returns although not as strongly as for the π-mode.

IV. CONCLUSIONS

The Englesberg-Schrieffer-like structure in the ARPES data of BISCO is consistent with the existence of an Einstein-like mode with $\Omega_0 \sim 40$meV coupled to the electrons as suggested by various authors.[34,35,36] However, it seems that it will be difficult to determine the origin of the mode based solely upon the (q_x,q_y) momentum dependence of its coupling. One might have thought that the q-dependence of the coupling or in the case of the π mode, the q-dependence of the resonance that has been parameterized as a q-dependent coupling, would give rise to clearly identifiable structure in $A(k,\omega)$. However, all of the modes show quite similar characteristic features at energies $\Omega_0+\Delta_0$ and $\Omega_0+E(0,\pi)$, which appear throughout the zone.

It would appear that the best place to look for a feature that could distinguish between, for example, the buckling phonon mode and the π-resonant mode is near the $k=(0,\pi)$ point. Here, the strong coupling of the π mode to the electrons for q near (π,π) leads to a secondary peak onsetting at an energy $\omega = -(E(0,\pi)+\Omega_0)$. For the buckling phonon mode, the coupling at $q=(\pi,\pi)$ vanishes and there is only a relatively weak response in this same frequency range. However, as we have seen, there is a secondary peak for the breathing mode which has nearly the same strength as that for the π-mode. Thus, the observed peak-dip-hump structure could also be consistent with a coupling to the oxygen-breathing mode. Recently, it has been suggested that the q_z dependence for a bilayer system may identify the mode as having $q_z = \pi$, which would provide support for the π resonance.[37] However, further work on the odd and even bilayer phonon coupling is needed for comparison.

While the coupling to the π-resonance mode along with a higher energy continuum spin-fluctuation spectrum provides an attractive unified framework, our results leave open the possibility that an oxygen phonon mode could also play a role. As we have seen, even with a relatively modest coupling constant $\lambda \sim 0.3$, one would expect to see evidence of some oxygen phonon modes. If they are not seen, then this suggests that the strong Coulomb many-body effects act to suppress the electron-phonon coupling. Alternatively, if it can be shown that the π-mode is not viable, oxygen phonon modes could provide a source for the resonant mode features. The continuum spin fluctuations would, of course, also contribute in this mixed scenerio. Here we should note that even if the mode were identified as the buckling mode, we find that its contribution to the magnitude of the $d_{x^2-y^2}$ gap is negligible because the increase in Z_1 more than offsets the increase in ϕ_1 (in Eq. (4) the d-wave coupling term is only 1/4 of the uniform coupling). This is in agreement with the results of Eliashberg-like T_c calculations[38] which find that, while the buckling phonons can provide an attraction in the $d_{x^2-y^2}$-channel, its contribution to Z leads to an overall reduction in T_c.

To conclude, from the results that we have found, it seems likely that the identification of the excitation responsible for the structure in the ARPES data will be decided on grounds other than the momentum dependence of the effective coupling. One aspect that remains under discussion is the strength of the various couplings. For the O phonon modes, LDA calculations[30,31] find intermediate coupling strengths with $\lambda \sim 0.3$ to 0.5. From our calculations it would appear that at this strength, one should in fact see structure in $A(k,\omega)$. If this is not seen, it raises the question of why is the electron-phonon coupling weakened in strongly-correlated materials?[16,22] The coupling to the π-resonance mode would appear to raise the opposite problem. That is, if the π-resonance mode is responsible for the Englesberg-Schrieffer-like signature in the ARPES spectrum, how can it be coupled so strongly?[15,23,24]

Acknowledgments

We would like to thank Z.-X. Shen for discussing his data with us, for his physical insights, and his enthusiasm for this project. DJS would also like to also acknowledge very useful discussions with S.V. Borisenko, W. Hanke, and S.A. Kivelson. AWS would like to acknowledge support from the Academy of Finland under project No. 26175. DJS acknowledges support from the National Science Foundation under grant No. DMR02-11166.

---

[*] Electronic address: asandvik@abo.fi

[†] Electronic address: djs@vulcan2.physics.ucsb.edu

[‡] Electronic address: bickers@physics.usc.edu

[1] S. Martin *et al.*, Phys. Rev. B **41**, 846 (1990).

[2] J.P. Franck, in *Physical Properties of High T_c Superconductors IV*, ed. by D.M. Ginsberg, World Scientific, Singpore, p. 189 (1994).

[3] M.K. Crawford, *et al.*, Phys. Rev. B **41**, 282 (1990).

[4] C. Boulesteix, K. Hewitt, J.C. Irwin, J. Phys. Cond. Mat. **12**, 9637 (2000).

[5] R.M. Macfarlane, H. Rosen, and H. Seki, Sol. St. Comm. **83**, 343 (1992).

[6] R.J. McQueeney *et al.*, Phys. Rev. Lett. **82**, 628 (1999).

[7] N. Pyka *et al.*, Phys. Rev. Lett. **70** 1457 (1993).

[8] A. Lanzara *et al.*, Nature **412**, 510 (2001).

[9] Z.-X. Shen, A. Lanzara, S. Ishihara, and N. Nagaosa, Phil. Mag. B **82**, 1349 (2002).

[10] E.W. Carlson, V.J. Emery, S.A. Kivelson, and D. Orgad, *Concepts in High Temperature Superconductivity*, cond-mat/0206217.

[11] S. Englesberg and J.R. Schrieffer, Phys. Rev. **131**, 993 (1963).

[12] A. Damascelli, Z. Hussain, and Z.-X. Shen, Rev. Mod. Phys. **75**, 473 (2003).

[13] A. Kaminski *et al.*, Phys. Rev. Lett. **86**, 1070 (2001).

[14] M. Eschrig and M.R. Norman, Phys. Rev. Lett. **85**, 3261 (2000).

[15] M. Eschrig and M.R. Norman, Phys. Rev. B **67**, 144503 (2003).

[16] R. Zeyher and M.L. Kulic, Phys. Rev. B **53** 2850 (1996).

[17] J. Song and J.F. Annett, Phys. Rev. B **51**, 3840 (1995); *ibid.* **52**, 6930 (E) (1995).

[18] D.J. Scalapino, J. Phys. Chem. Solids **56**, 1669 (1995).

[19] A. Nazarenko and E. Dagotto, *Phys. Rev. B* **53**, R2987 (1996).

[20] T. Dahm, D. Manske, D. Fay, and L. Tewordt, Phys. Rev. B **54**, 12006 (1996).

[21] N. Bulut and D.J. Scalapino, Phys. Rev. B **54**, 14971 (1996).

[22] Z.B. Huang, W. Hanke, E. Arrigoni, and D.J. Scalapino; cond-mat/0306131. These Monte Carlo Calculations for a Hubbard model find that, while the electron-phonon vertex is suppressed at large momentum transfers, it can actually be enhanced at small momentum transfers. This latter effect differs from Ref. 16.

[23] H.-Y. Kee, S.A. Kivelson, and G. Aeppli, Phys. Rev. Lett. **88**, 257002 (2002).

[24] A. Abanov, A.V. Chubukov, M. Eschrig, M.R. Norman, and J. Schmalian, Phys. Rev. Lett. **89**, 177002 (2002).

[25] D.J. Scalapino and P.W. Anderson, Phys. Rev. **33**, A921 (1964).

[26] In the superconducting state the value of $Z_1(\Delta_0)$ is less than the normal state renormalization factor $1+\lambda = 1.5$ due to the additional energy associated with the gap. Traditionally, when Ω_0 was large compared to Δ_0, this effect was negligible. Here, however, since $\Omega_0 = 1.5\Delta_0$, the effective λ for the s-wave case is of order $2|g|^2N(0)/(\Omega_0+\Delta_0) = 0.6\lambda = 0.3$. For the d-wave case, the effective λ is also reduced but not quite as much because of the nodes. In the following, we will use $Z_1(k,\omega=0)$ at the nodal point to give the nodal Fermi velocity renormalization for the d-wave case.

[27] D.J. Scalapino, in *Superconductivity, Vol 1*, ed. by R.D. Parks, Marcell Dekker, New York (1969).

[28] J.E. Hoffman *et al.*, Science **295**, 466 (2002).

[29] We will address the important question of whether the magnetic resonance mode is in fact sufficiently strongly coupled to the quasi-particles to give the observed structure in a later paper. Different conclusions regarding this have been reached in Refs 23 and 24.

[30] O.K. Andersen, S.Y. Savrasov, O. Jepsen, and A.I. Liechtenstein, J. Low Temp. Solids **105**, 285 (1996).

[31] O. Jepsen, O.K. Andersen, I. Dasgupta, and S. Savrasov, J. Low Temp. Solids **59**, 1718 (1998).

[32] S.V. Borisenko *et al.*, cond-mat/0209435.

[33] T.K. Kim *et al.*, cond-mat/0303422.

[34] Z.-X. Shen and J.R. Schrieffer, Phys. Rev. Lett. **78**, 1771 (1997).

[35] M.R. Norman *et al.*, Phys. Rev. Lett. **79**, 3506 (1997).

[36] M.R. Norman and H. Ding, Phys. Rev. B **57**, R11089 (1998).

[37] M. Eschrig and M.R. Norman, Phys. Rev. Lett. **89**, 277005 (2002).

[38] T.S. Nunner, J. Schmalian, and K.H. Bennemann, Phys. Rev. B **59**, 8859 (1999).